Grain boundary motion and grain rotation in aluminum bicrystals: recent experiments and simulations

To cite this article: D A Molodov *et al* 2015 *IOP Conf. Ser.: Mater. Sci. Eng.* **89** 012008

IOP Conf. Series: Materials Science and Engineering **89** (2015) 012008 doi:10.1088/1757-899X/89/1/012008

Grain boundary motion and grain rotation in aluminum bicrystals: recent experiments and simulations

DA Molodov, LA Barrales-Mora and J-E Brandenburg
Institute of Physical Metallurgy and Metal Physics, RWTH Aachen University, D-52056 Aachen, Germany

E-mail: molodov@imm.rwth-aachen.de

Abstract. The results of experimental and computational efforts over recent years to study the motion of geometrically different grain boundaries and grain rotation under various driving forces are briefly reviewed. Novel in-situ measuring techniques based on orientation contrast imaging and applied simulation techniques are described. The experimental results obtained on specially grown aluminum bicrystals are presented and discussed. Particularly, the faceting and migration behavior of low angle grain boundaries under the curvature force is addressed. In contrast to the pure tilt boundaries, which remained flat/faceted and immobile during annealing at elevated temperatures, mixed tilt-twist boundaries readily assumed a curved shape and steadily moved under the capillary force. Computational analysis revealed that this behavior is due to the inclinational anisotropy of grain boundary energy, which in turn depends on boundary geometry. The shape evolution and shrinkage kinetics of cylindrical grains with different tilt and mixed boundaries were studied by molecular dynamics simulations. The mobility of low angle <100> boundaries with misorientation angles higher than 10°, obtained by both the experiments and simulations, was found not to differ from that of the high angle boundaries, but decreases essentially with further decrease of misorientation. The shape evolution of the embedded grains in simulations was found to relate directly to results of the energy computations. Further simulation results revealed that the shrinkage of grains with pure tilt boundaries is accompanied by grain rotation. In contrast, grains with the tilt-twist boundaries composed of dislocations with the mixed edge-screw character do not rotate during their shrinkage. Stress driven boundary migration in aluminium bicrystals was observed to be coupled to a tangential translation of the grains. The activation enthalpy of high angle boundary migration was found to vary non-monotonically with misorientation angle, whereas for low angle boundaries the migration activation enthalpy was virtually the same. The motion of the mixed tilt-twist boundaries under stress was observed to be accompanied by both the translation of adjacent grains parallel to the boundary plane and their rotation around the boundary plane normal.

1. Introduction

The grain microstructure of crystalline solids decisively determines their physical and mechanical properties. Grain boundaries, i.e. interfaces between crystallites of the same phase with different crystallographic orientations, have the unique property to react to applied forces by their displacement. Grain boundary migration, by which the crystalline solid is reconstructed atom by atom, as well as grain rotation are essential parts of grain microstructure evolution in polycrystals during plastic deformation and in the course of recrystallization and grain growth during annealing at elevated temperatures.

It is commonly accepted that grains rotate towards a low energy grain boundary configuration associated with the low Σ CSL orientation relationships [1-3]. This was confirmed by atomistic computer simulations by several groups [4-6]. According to the theoretical model by Cahn and Taylor [7], grain rotation can be induced by grain boundary motion due to the coupling between boundary motion and tangential translation of the adjacent grains, which is proportional to the normal boundary displacement. Since Cahn and Taylor have proposed their approach to describe grain boundary motion, grain translation and grain rotation [7], significant progress was achieved with respect to the theoretical analysis of the shear-migration coupling [8-15]. Also, a substantial body of experimental evidence of this phenomenon was obtained for planar boundaries [16-23]. Further, it has been experimentally shown that stress driven boundary migration can be accompanied by grain rotation [24].

The motion of grain boundaries is controlled by their mobility m and the applied driving force p. As was predicted theoretically [25,26] and shown by numerous experiments [16,27-31], the rate of boundary migration v is proportional to the acting driving force

$$v = mp \tag{1}$$

The grain boundary mobility can be extracted from the temporal change of the grain size during annealing, since polycrystals are always liable to grain growth owing to a driving force arising from the curvature of the grain boundaries. The large part of the grain boundary mobility data was derived just from such kind of experiments. However, measurements of boundary mobility based on the change of the mean grain size with time in polycrystals give only a mean value, averaged over many different types of grain boundaries. Specific data on grain boundary mobility can only be obtained from the behavior of individual boundaries with well-defined geometry. This can be accomplished in experiments on specially grown bicrystal.

It is well established that both grain boundary energy and mobility to a great extent depend on grain boundary character, which is commonly reduced to misorientation between neighboring grains and inclination of the boundary plane [32]. A dependence of grain boundary energy on inclination can result in the formation of low energy grain boundary facets [33-40], which in turn can substantially affect grain boundary motion [41-45] and, therefore, be crucial for processes of microstructural evolution in polycrystals [46-50].

It is widely accepted that grain boundary faceting relates to high angle boundaries with misorientations close to low Σ CSL orientation relationships [33-36]. It has been, however, experimentally proved that the same behavior also applies to low angle tilt grain boundaries with low index rotation axis [51-54]. In experiments on aluminum bicrystals with <100> and <111> tilt grain boundaries with misorientation angles θ in the transition range from low to high angles it was found that, in contrast to expectations for the used bicrystal geometry (Fig. 1), only boundaries with misorientation angles larger than 15° could assume a curved shape and steadily move under a capillary driving force. Low angle boundaries ($\theta < 15°$) did not assume a continuously curved shape [55] and, correspondingly, did not move under a capillary driving force [51-54]. In the entire investigated temperature range they remained flat or formed facets which met the initial boundary at a sharp edge (e.g. Fig. 5 in Ref. [52]). The observed faceting behavior of tilt grain boundaries and its change with increasing misorientation was attributed to the dependence of grain boundary energy on inclination [51,52].

It is important to note, however, that a geometrically pure tilt grain boundary with a low index rotation axis is a specific model case. Actually, most previous experimental and modeling studies of grain boundary dynamics were performed on tilt boundaries [32], since they are easier to fabricate in both experiment and simulations. In a real polycrystal most boundaries are not pure tilt or pure twist but rather of general type. Their structure is more complex than that of pure tilt boundaries, which are composed of edge dislocations. Therefore, the migration and faceting behavior of random grain boundaries can be expected to differ substantially from that of pure tilt boundaries. Also, the dynamic/rotation behavior of grains with random boundaries can be very different from that of grains with pure tilt boundaries. In the current paper the results of experimental and computational efforts

over recent years to study the motion of geometrically different grain boundaries and grain rotation under various driving forces are briefly reviewed.

2. Applied driving forces and measuring techniques

The experiments were conducted on specimens (Fig. 1) fabricated by electro-discharge machining from high purity Al bicrystals (99.9995%) grown by the vertical Bridgman technique. Details of the crystal growth, bicrystal characterization and sample preparation are given elsewhere [16-18,51,52].

2.1. Boundary migration under a curvature driving force

The well approved experimental technique [51-63] for measuring grain boundary migration under a constant curvature driving force p_c provided by the boundary energy γ, $p_c = \gamma/a$ (Fig. 1) was applied. Grain boundaries with various rotation angles around a <100> axis and different orientations of this axis with respect to the boundary plane and sheet normal were examined. The investigated mixed tilt-twist grain boundaries were composed of a rotation angle θ around a common [001] axis and grain boundary plane rotated by an angle $\xi \approx 20°$ with respect to the tilt boundary plane (Fig. 1a). The angle ξ, therefore, specifies a twist component of a mixed grain boundary. In particular, <100> mixed boundaries with misorientations 4.9°, 9.1°, 12.3° and 20.9° were investigated. For comparison the behavior of a 9.1° [001] pure tilt boundary, i.e. with $\xi = 0°$, was also examined. In two further investigated bicrystals with 7.0° and 11.4° $[\bar{1}00]$ boundaries a common rotation axis of the adjacent grains was parallel to the bicrystal surface as shown in Fig. 1b. The initial inclination of a 7.0° $[\bar{1}00]$ boundary was parallel to the growth (x -) axis of the bicrystal, i.e. this boundary had tilt geometry. The plane of the 11.4° $[\bar{1}00]$ boundary was initially inclined from the pure tilt position by about 6° (rotated around z-axis), i.e. it was of a mixed geometry with a twist component $\xi = 6°$.

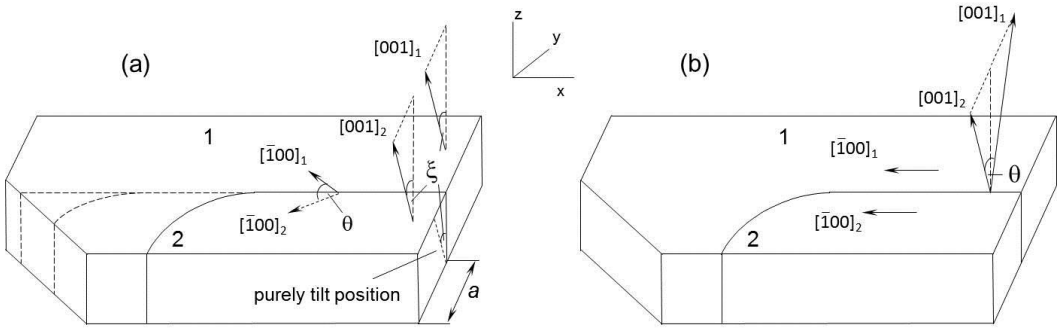

Figure 1 Bicrystal geometries for measuring the grain boundary migration. (a) Bicrystal with a θ <100> tilt-twist grain boundary (ξ is a twist component); (b) bicrystal with a θ <100> tilt boundary with a rotation axis parallel to the specimen surface [54].

The measurements of grain boundary shape and motion in the temperature range between 390°C and 640°C were performed by an in-situ technique in a SEM equipped with a specially designed heating stage [64]. The grain boundary shape and location were determined utilizing the orientation contrast revealed by a secondary electron detector (Fig. 5). The measuring procedure is described in Refs. [51,52].

2.2. Stress-induced grain boundary migration

Grain boundaries can also be driven by an applied mechanical stress. For a tilt grain boundary with misorientation angle θ subjected to shear stress τ the migration driving force p_s can be expressed as [65]

$$p_s = 2\tau cos\varphi \cdot tan(\varphi/2) \quad (2)$$

where $\psi/2$ is the angle between the grain boundary normal and the effective Burgers vector $\boldsymbol{b}$ per unit boundary length as determined from the Frank-Bilby equation [8,9]. For example, for <100> tilt boundaries $\varphi = \theta$ for the <100> mode of migration-shear coupling and $\varphi = \theta - 90°$ for the <110> coupling mode [8,9]. For low angle <100> tilt boundaries, for which φ is small or close to 90° Eq. (2) can be approximated by [16]

$$p_s \approx \tau sin\varphi \tag{3}$$

The recent measurements of stress induced grain boundary migration [19-21,24,66,67] were performed by in-situ observations and recording of grain boundary migration using a hot deformation stage integrated in a SEM [19,66].

For an application of a shear stress to the grain boundaries two sets of grips were designed and fabricated (Fig. 2). Each pair of the grips is applicable to specimens with a particular geometry. Grain boundary behaviour under an applied stress can be observed and measured in-situ utilizing the orientation contrast on the specimen surface revealed by a secondary electron detector (Fig. 3). An analysis of the recorded orientation image sequences with a special software reveals the normal boundary displacement d and the lateral grain translation s.

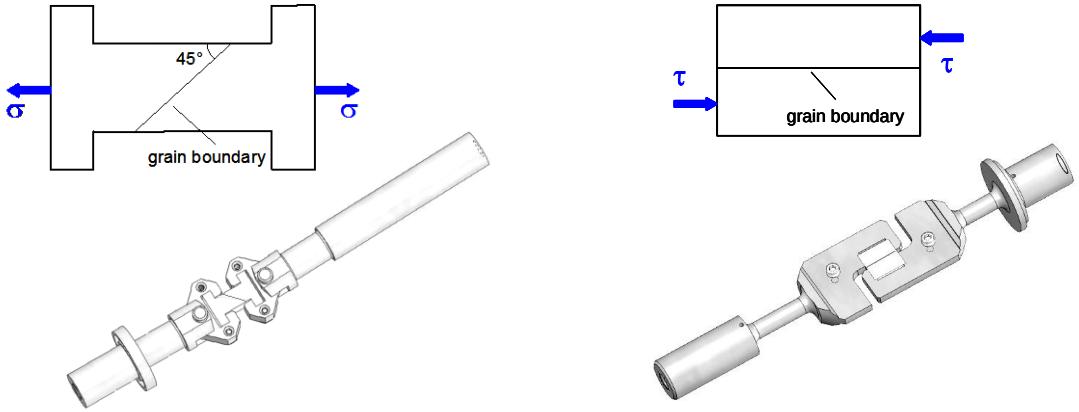

Figure 2 Bicrystal geometry and corresponding grips for the application of a shear stress to the grain boundary [19].

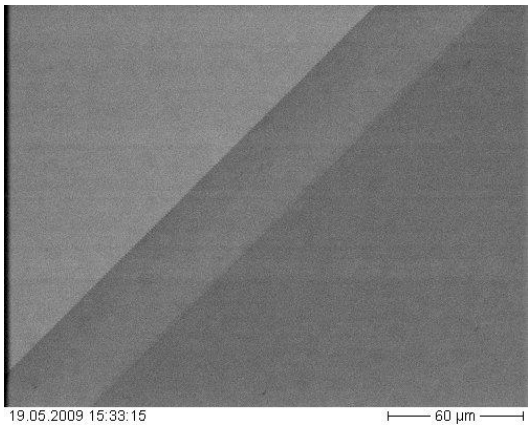

Figure 3 Motion of a 76.4°<100> tilt grain boundary in an Al bicrystal under an applied tensile stress of 0.26 MPa during annealing at 380°C.

3. Applied modeling techniques

In order to determine the grain boundary energy of both the <100> tilt and mixed grain boundaries the computation procedure proposed by Lee and Choi [68] was applied. The method does not require periodic boundary conditions, typically assigned to the simulation sample in the two directions parallel to the boundary and, thus, can be utilized for computing grain boundary energy for any misorientation and inclination angles. The second nearest-neighbor modified embedded atom method (2NN MEAM) potential for Al developed by Lee et al. [68-71] was utilized to describe the interaction between atoms. The energy of the created bicrystal sample was subsequently minimized by application of 0K molecular statics. The grain boundary energy was determined as the difference between the computed potential energies of the bicrystal and the original single crystal sphere [54].

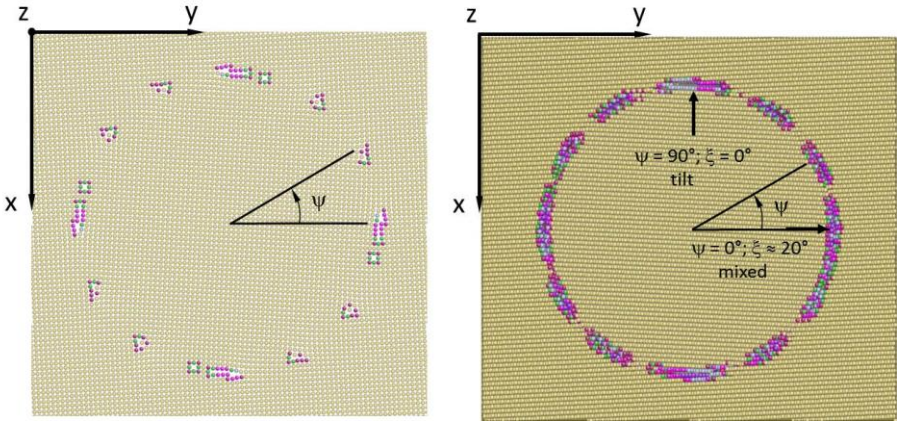

(a) **(b)**

Figure 4 Cross-sections of the simulation box with the embedded cylindrical grain with the 5.5°<100> (a) tilt and (b) mixed tilt-twist boundary. The grain and the matrix are rotated by $\pm\ \theta/2$ (here θ_0=5.45°) around the common [100] axis, which (a) for grain with the pure tilt boundary is aligned parallel to the z axis and for grain with the mixed boundary is tilted by an angle $\xi \approx 20°$ around the x axis.

In order to analyze the effect of the inclinational anisotropy of grain boundary energy on the grain shape evolution and grain growth kinetics molecular dynamics (MD) simulations were employed. The large-scale atomic/molecular massively parallel simulator (LAMMPS) code [72] was utilized. The atomic interactions were described by the same 2NN MEAM potential as employed in the molecular statics (MS) simulations. The configuration used in these MD simulations was composed of a cylindrical grain embedded in a differently oriented crystalline matrix. The capillary driven shrinkage of such a grain misoriented with respect to the matrix by different angles θ around a common <100> axis was studied. Four pairs of grains with pure tilt and mixed tilt-twist boundaries (Fig. 4) with the misorientation angles θ_0= 5.45°, 10.38°, 16.26°, and 22.61° were examined. The grains with tilt boundaries were misoriented around the [100] axis aligned parallel to the z axis of the simulation box (Fig. 4a). The boundaries of these grains retain their pure tilt character over the entire circle/length. For computing the grains with the mixed boundaries the common [100] rotation axis was additionally rotated counterclockwise by an angle of about $\xi \approx 20°$ ($\xi \equiv \mathrm{acos}([100] \cdot \bar{c}/||c||)$) around the crystallographic direction parallel to the x axis of the simulation box. At the inclination $\psi = 0°$, therefore, these boundaries had a tilt-twist character with a 20° twist component. With increasing inclination ψ the twist component ξ decreases down to zero at $\psi = 90°$ (Fig. 4b). All simulations were performed at 400°C. Grain rotation during shrinkage was not prohibited to allow the natural development of the system. The change of the grain volume with time was tracked by using an orientation dependent order parameter for the atoms, as defined in [73].

4. Faceting and migration behavior of low angle boundaries of different character

The experiments revealed that all investigated mixed <100> tilt-twist grain boundaries readily assumed a continuously curved shape (Fig. 5) and while migrating retained their shape self-similar in the entire investigated temperature range. All boundaries moved steadily at constant temperature (Fig. 6a), such that the velocity v for each temperature could be calculated. From the obtained boundary velocity the reduced mobility A was determined as

$$A \equiv v \cdot a = A_0 exp(-H/kT) = m\gamma \quad (4)$$

where a is the width of the shrinking grain (Fig. 1), H is the activation energy and A_0 the pre-exponential factor. The temperature dependence of the reduced mobility for all investigated mixed boundaries is shown in Fig. 6b.

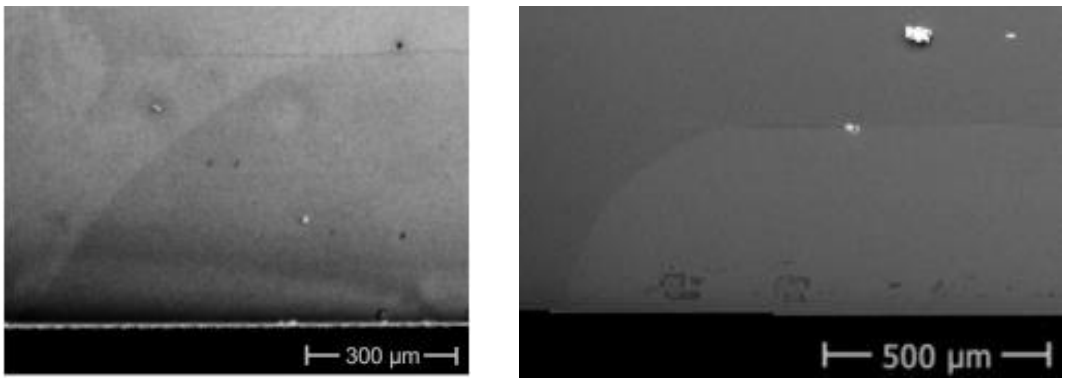

(a) **(b)**

Figure 5 Images of the moving mixed tilt-twist grain boundaries during annealing at elevated temperatures. (a) 4.9°<100> (twist component $\xi \approx 20°$) (Fig. 1a); (b) 11.4°<100> boundary, which in the original straight configuration (Fig. 1b) had a twist component of $\xi \approx 6°$.

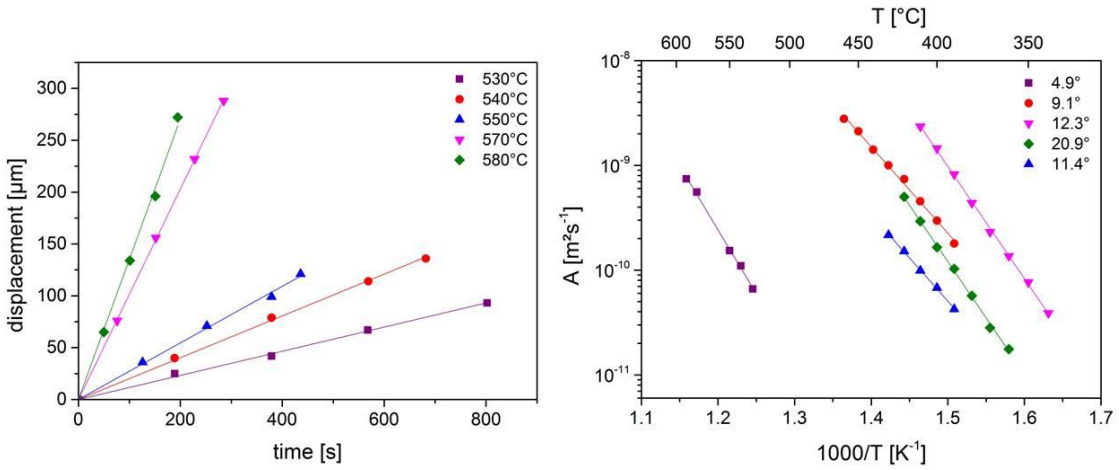

(a) **(b)**

Figure 6 (a) Displacement vs. time at various temperatures for migration of a 4.9°<100> mixed boundary; (b) Reduced mobility, i.e. boundary velocity v, normalized by the reciprocal width of the shrinking grain, a^{-1} (see Eq. (4)), vs. temperature for the migration of the investigated <100> mixed boundaries.

In contrast to the behavior of the mixed <100> boundaries, the 9.1° and 7.0° <100> pure tilt boundaries (with geometry shown in Fig 1a and 1b, respectively) did not assume a curved shape. They

remained straight and, therefore, did not move during annealing at elevated temperatures up to 640°C. These observations are consistent with the results of previous experiments on low angle <100> and <111> tilt boundaries [51,52]: the boundary remained flat and did not move under the driving force provided by its energy. Obviously, this is due to the anisotropy of its energy with respect to boundary inclination (Fig. 7). In the original position both the 9.1° and 7.0° boundaries have a local minimum energy at the symmetrical configuration with $\psi = 0°$ (as 10.4° <100> pure tilt boundary in Fig. 7). Accordingly, due to their minimal energy the symmetrical 9.1° and 7.0° tilt boundaries retained the initial flat/faceted configuration and, therefore, did not move under the driving force provided by their energy.

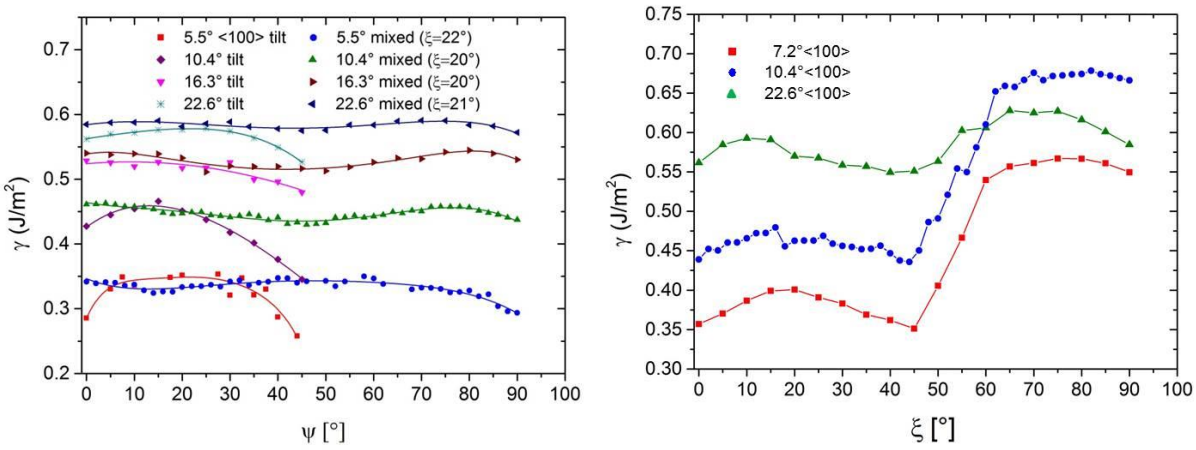

(a) **(b)**

Figure 7 Computed dependence of the grain boundary energy (a) on boundary inclination for <100> tilt and mixed (twist component $\xi \approx 20°$) boundaries and (b) upon change of the boundary geometry from pure <100> tilt ($\xi = 0°$) to pure <100> twist ($\xi = 90°$) at 0 K.

As revealed by MS simulations, the change of the boundary geometry from pure tilt to mixed tilt-twist resulted in an essential change of the inclination dependence of the boundary energy. As seen in Fig. 7a, the energy of the mixed grain boundaries is essentially constant throughout the entire inclination range. As a result, according to the tendency of the system to minimize the total boundary area, the initially straight boundary configuration can easily be replaced by a continuously curved boundary shape that allows the boundary to move under a capillary driving force during heating at elevated temperature, as observed in the experiments (Fig. 5).

The computed inclination dependence of grain boundary energy $\gamma(\xi)$ in Fig. 7b provides the explanation of the behavior of 11.4° mixed boundary (see Fig. 1b), which in contrast to 7.0° tilt boundary became curved and mobile (Fig. 5b). The energy of the investigated 11.4° <100> mixed boundary in its original position with $\xi = 6°$ is already outside the energetic minimum at the pure tilt position with $\xi = 0°$. This is obviously high enough to avoid the faceting (retaining the origin straight configuration) during annealing at elevated temperatures.

5. Grain shape evolution during shrinkage of initially cylindrical grains with boundaries of different character

The computed temporal evolution of the shape and size of the shrinking initially circular grains with different boundaries was found to depend on both the misorientation angle and character of the examined boundaries [54]. Very soon after the beginning of the respective simulation runs the grains with low angle 5.5° and 10.4° tilt boundaries assumed a faceted shape with well pronounced flat sides with inclinations close to $\psi = 0°/90°$ and $\psi = 45°$ (Fig. 8). The grain with the 16.3° tilt boundary was

much more rounded but observed to form non-stable facets appearing and disappearing during the grain shrinkage. In contrast, the shapes of the grains with the same misorientations with respect to the matrix but mixed tilt-twist boundaries were observed to be essentially rounded. The grains with the high angle 22.6° boundaries both tilt and mixed were well rounded close to a circle during shrinkage [54].

Apparently, the results of MD simulations are in direct relation to the results of MS simulations. The formation of a faceted octagon-like shape of grains with low angle 5.5° and 10.4° tilt boundaries can be rationalized in terms of the essential inclinational anisotropy of their energy revealed by MS simulations. The flat sides of these grains represent symmetrical boundary configurations with inclinations ψ = 0°/90° and ψ = 45°, where the energy attains distinct minima (Fig. 7a). A closer inspection of the shape of grains with low angle tilt boundaries (after 1 ns computational annealing) revealed that they comprise eight symmetrical boundary facets, which in turn are composed of edge dislocations with Burgers vectors b = a<100> and a/2<110> [54]. The formation of a faceted shape of grains with low angle tilt boundaries in MD simulations also conforms to the behavior of a 9.1° pure tilt boundary observed in the experiment, where this boundary remained straight in the whole temperature range investigated.

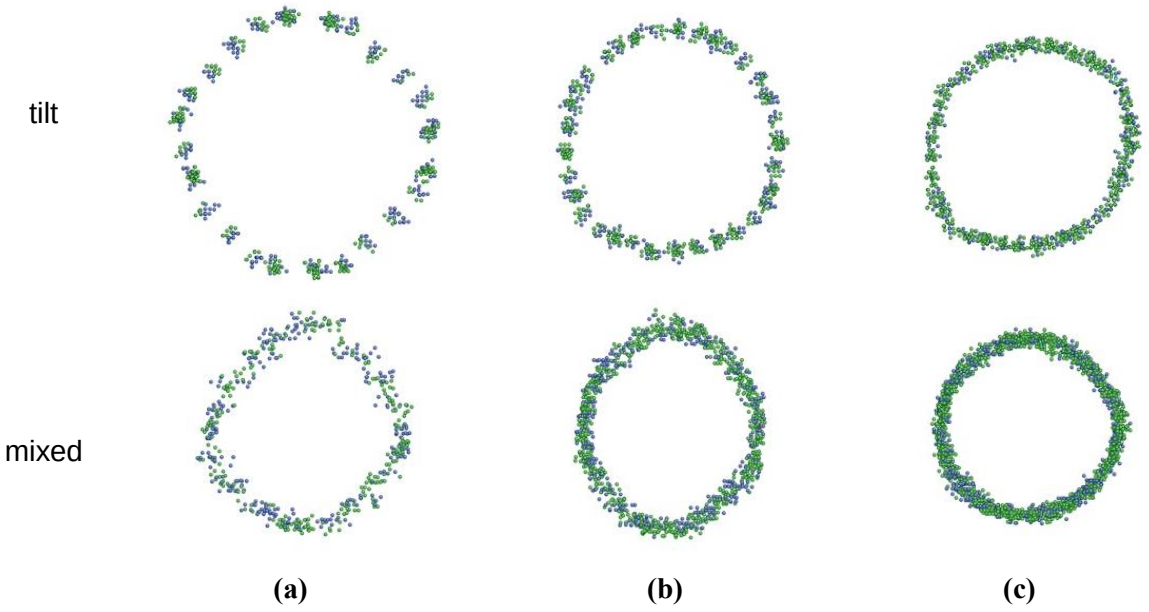

Figure 8 Snapshots of MD simulations of shrinking initially cylindrical grains with tilt and tilt-twist character at equal time of shrinkage t = 1.01 ns. (a) 10.4°; (b) 16.3°; (c) 22.6°. The grain boundaries are revealed by displaying only atoms with a coordination number z = 10 and z = 13.

As revealed by MD simulations, in contrast to grains with low angle tilt boundaries, the grains with 16.3° and 22.6° tilt boundaries shrank keeping their round shape (Fig. 8). This is obviously due to a reduction of inclinational anisotropy of grain boundary energy with increasing misorientation, which is well seen in Fig. 7 by comparing the $\gamma(\psi)$ dependency for the investigated boundaries. Furthermore, the almost isotropic energy of mixed low angle boundaries revealed by MS simulations (Fig. 7a) seems to account for the formation of a rounded shape of grains with 5.5° and 10.4° mixed boundaries as observed in MD simulations. As discussed above, for the same reason the experimentally examined 12.3°, 9.1° and 4.9° mixed grain boundaries, in contrast to the 9.1° pure tilt boundary, could readily assume the curved shape and move under the capillary driving force.

6. Mobility of <100> low angle boundaries

The results of the measurements of low angle <100> mixed boundary motion [54] revealed that the mobilities of boundaries with relatively high misorientations (9.1°, 11.4° and 12.3°) essentially did not differ from that of the 20.9° boundary and those of high angle tilt boundaries, which due to their sufficiently isotropic energy are capable to move having pure tilt geometry. This is particularly apparent in Fig. 9a, where the mobilities of the investigated boundaries at 410°C are shown together with the data for high angle 18.3°, 20.0° and 23.5° <100> tilt boundaries in Al bicrystals of the same purity obtained previously [52]. As seen, the mobilities obtained for low angle boundaries with $\theta > 9°$ are in the range of values, which are typical for high angle <100> boundaries.

In contrast, the 4.9° boundary in our experiments moved with similar velocities as the other boundaries only at substantially higher temperatures between 525°C and 590°C (Fig. 6b). Consequently, at a given temperature it is comparatively much less mobile. As seen in Fig. 9a, its mobility interpolated to the temperature of 410°C is about three orders of magnitude lower than that of the other (low angle mixed and high angle tilt) boundaries. This result is in a good agreement with the data obtained in experiments on Al polycrystals [74,75] as well as measurements on Cu bicrystals [76].

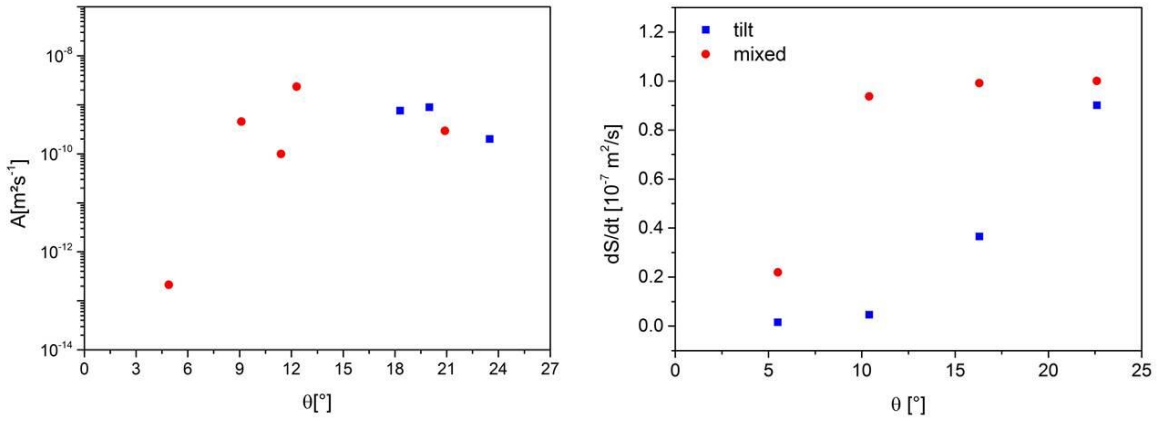

(a) **(b)**

Figure 9 (a) Reduced mobility $A = v \cdot a$ of investigated <100> mixed tilt-twist boundaries (circle symbols) at 410°C. The square symbols represent data obtained for the migration of high angle <100> pure tilt boundaries with misorientations 18.3°, 20.0°, 23.5° in Al bicrystals of the same purity at the same temperature [52]. (b) Misorientation dependence of the computed rate of grain area change dS/dt as obtained in MD simulations.

Figure 9b shows the rate of grain area change dS/dt with growing misorientation θ for all tilt and tilt-twist boundaries as obtained in MD simulations. For both types of boundaries the rate of grain area change was found to increase with misorientation, although in different ways. For low angle (5.5° and 10.3°) tilt boundaries it did not differ significantly, but rose much faster with a further increase of θ. It can be understood, taking into account that both the lower energy γ of low angle boundaries and the smaller local curvature κ of most boundary segments of these grains (due to the faceting) caused a reduction of the capillary driving force $p_c = \gamma\kappa$. The grain with the 5.5° mixed boundary shrank faster, but not substantially faster, than that with the 5.5° tilt boundary. With an increase of misorientation from 5.5° to 10.3°, however, the rate of area change for a grain with the mixed boundary increased very rapidly up to the level of dS/dt values for grains with the medium angle 16.3° and high angle 22.6° mixed boundaries (Fig. 9b).

It is remarkable that the both computed misorientation dependence of dS/dt and dependence $A(\theta)$ obtained in experiments (Fig. 9) are qualitatively similar. In both the experiments and MD simulations the low angle <100> mixed boundaries with a misorientation angle around 10° were found to be quite

mobile with the mobility similar to that of <100> high angle boundaries (no matter tilt or mixed). Also, akin to experiments, the simulations revealed that with decreasing misorientation down to about 5° the boundary mobility decreases substantially.

7. Rotation behavior of grains with pure tilt and mixed <100> boundaries

The remarkable result of the MD simulations performed is that they revealed the crucial impact of grain boundary character on a grain rotation during shrinkage [54,77]. The simulated grains with pure tilt boundaries rotated towards higher θ, while grains with the mixed tilt-twist boundaries practically did not rotate during their shrinkage. This is illustrated in Fig. 10, where snapshots of the grains with misorientation angles θ_0= 16.26° and 22.61° after their shrinkage down to the normalized grain volume of V/V_0= 0.25, where V_0 is the initial grain volume, are depicted.

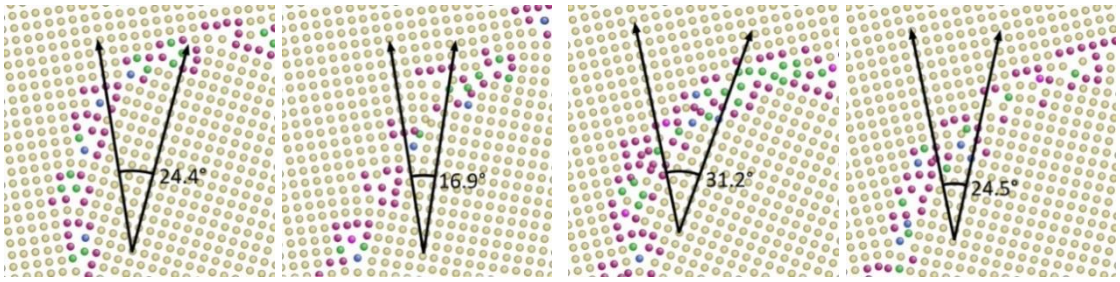

(a) **(b)**

Figure 10 Grain misorientation and grain boundary structure as observed on (100) crystallographic planes for grains with the (a) θ_0= 16.26° and (b) θ_0= 22.61° tilt and mixed boundaries (left and right, respectively) after grain shrinkage to V/V_0= 0.25 (V and V_0 are a shrinking and initial grain volume, respectively).

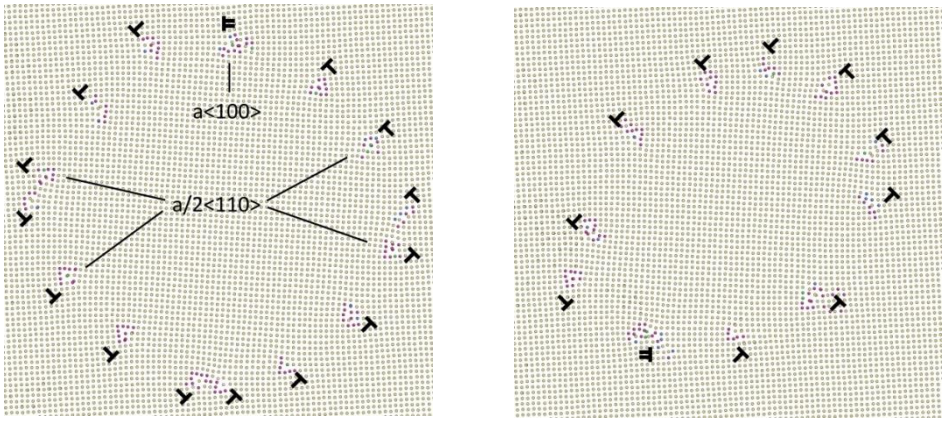

(a) **(b)**

Figure 11 Dislocation structure of the grain boundary with θ_0= 5.45° as it appears on a {100} crystallographic plane after annealing for (a) 0.11 ns and (b) 0.42 ns. Atoms are colored according to their coordination number [77].

The observed rotation of grains with tilt boundaries can be understood in terms of the grain boundary motion coupled to shear [7,8]. The grain rotation induced by grain boundary motion was analyzed theoretically [7] and observed in computer simulations [78-80]. According to the model [7],

the grain rotation caused by the boundary motion perfectly coupled to shear is characterized by the conservation of the dislocation content of the boundary and, therefore, rotation of the shrinking grain towards higher θ is associated with the substantial increase of the dislocation density in the grain boundary. This case is obviously applied to the results of our MD simulations performed for grains with pure tilt boundaries composed of edge dislocations.

On the other hand, the grains with mixed boundaries were observed not to rotate during their shrinkage [54,77]. The dislocation content of these boundaries, therefore, was not characterized by the invariant dislocation number, but rather by the constant dislocation density that preserved essentially the grain boundary structure. This behavior requires an effective annihilation of grain boundary dislocations. Indeed, a closer inspection of the atomic configurations in the boundary revealed that dislocations with the mixed edge-screw character, which compose the respective boundaries, can easily interact with each other and annihilate as a result of the chains of dissociation and recombination reactions (Fig. 11) [77].

Therefore, the results of the performed MD simulations distinctly demonstrated a sensitivity of grain rotation during curvature driven grain shrinkage on grain boundary structure. The availability of the effectively operating mechanisms of dislocation annihilation in the mixed grain boundaries, for instance as identified in Ref. [77], was the most likely reason for the missing rotation during shrinkage of the island grains in thin films of Al [81] and Au [82,83], where grain boundaries were not of ideally pure tilt character with low index rotation axis.

Obviously, based on the simulation results obtained for the three investigated pairs of orientation relationships, it is impossible to conclude about the possibility of rotation of grains with all various boundary structures. However, it can be suggested that if the further studies will confirm the confinement of grain rotation during capillarity driven shrinkage to grains with pure tilt boundaries only, this phenomenon can be considered as playing a minor role for microstructure development during grain growth in conventional polycrystals, but can be probably appreciable in the development of sharply textured columnar structures.

8. Mechanically induced grain boundary migration and grain rotation

Stress driven grain boundary motion was predicted theoretically by Read and Shockley for low angle symmetrical tilt boundaries [84] and first experimentally observed for low angle boundaries in Zn [85-87]. It has been found, also in experiments with some high angle boundaries with low Σ CSL relationships in bicrystals of Al, Zn and ZrO_2 [88-95], that boundary migration under an applied shear stress is coupled to a strain, which in bicrystals is observed as a translation of the grains parallel to the boundary plane. According to the common understanding based on these observations, the coupled boundary migration is confined to symmetrical low angle boundaries composed of edge dislocations and special low Σ high angle boundaries comprising secondary grain boundary dislocations: the dislocation glide under stress leads to a shear deformation of the crystal region swept by the moving boundary. According to the dislocation model of low angle tilt grain boundaries by Read and Shockley [84], for symmetrical low angle tilt boundaries the relation between normal boundary displacement d and grain translation s, also referred to in literature as coupling factor $\beta = s/d$ (Fig. 12), changes with misorientation angle θ according to the tangent rule $\beta = 2tan(\theta/2)$. More recent theoretical models [8-12] predict that the boundary migration-shear coupling can occur for high angle boundaries as well. This has been also confirmed by computer simulation studies [10,96-99] and observed for random boundaries by TEM investigations in nanocrystalline and ultrafine-grained polycrystals [100-102].

8.1. Experimental proof of boundary migration-shear coupling

In a series of experiments [16-18] the stress-driven migration of planar symmetrical <100> tilt boundaries with misorientations in the entire angular range (Fig. 13) was measured. It has been proved that stress driven grain boundary motion is coupled to a shear strain of the crystal region behind the moving boundary. The important result of these experiments with various <100> tilt boundaries is that

contrary to the common understanding the boundary migration – shear coupling is not confined to low angle and some low Σ high angle boundaries, but is a typical observation for any symmetrical <100> tilt boundaries in the entire range of misorientations between 0° and 90°, no matter how close to low Σ CSL orientation relationships. Moreover, the experimental results have verified the prediction of the model by Cahn et al. [8,9] that the tangent rule for calculation of the coupling factor β retains its validity over the entire misorientation range including the high angle regime: as depicted in Fig. 13a, the values of the coupling factor calculated according to the model are in excellent agreement with the values obtained in the experiment. Two branches in the misorientation dependence of the coupling factor in Fig. 13a confirm that for <100> tilt boundaries there are indeed two geometrically different mechanisms of shear-coupled boundary migration [8], which can formally be represented by slip of dislocations with Burgers vector b=a<010> on a {001} plane or b=a/2<110> on {110}, respectively.

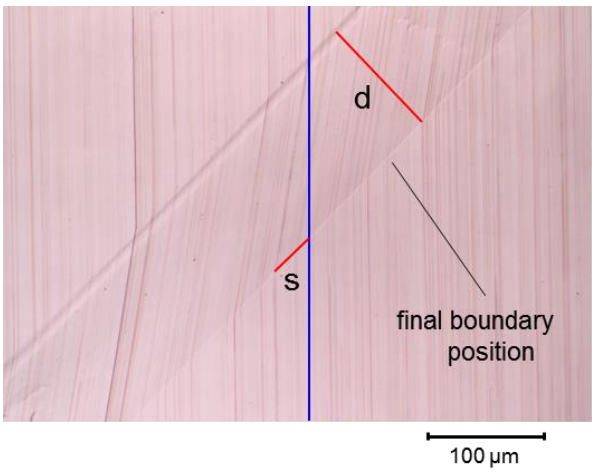

Figure 12 Migration-shear coupling of a 23.6°<111> tilt boundary moving under a tensile stress of 0.34 MPa (after 30 minutes annealing at 340°C) [18]. Coupling between grain boundary migration and produced shear is characterized by the factor determined as $\beta = \gamma = s/d$. The measured β for the 23.6°<111> tilt boundary is β = 0.42, which is equal to the theoretical value β_{theor}.

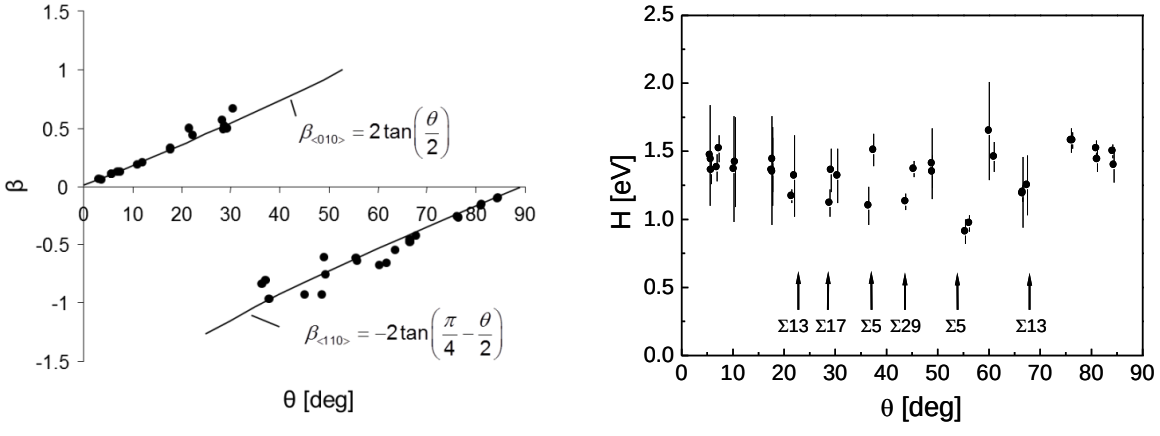

(a) **(b)**

Figure 13 (a) Measured (points) and calculated (lines) coupling factors β and (b) activation enthalpy H of stress driven migration vs. misorientation angle θ for symmetrical <100> tilt grain boundaries [18].

The boundary migration – shear coupling was observed not only for symmetrical but also for asymmetrical tilt grain boundaries. The structure of asymmetrical low angle boundaries is represented by a mixed arrangement of dislocations with different Burgers vectors. Particularly, asymmetrical <100> tilt boundaries consist of dislocations with both a<010> and a/2<110> Burgers vectors. Under a stress these dislocations should move on different planes. According to Read and Shockley [84] this renders their concurrent motion impossible without hindering and locking each other. Consequently, asymmetrical tilt boundaries in the dislocation model cannot be driven by a stress and, therefore, cannot cause a shape change of a bicrystal. Contrary to this prediction, the experiments with <100> tilt boundaries [20] as well as measurements on bicrystals with <111> tilt boundaries [67], showed that the asymmetrical tilt boundaries can move under an applied stress and produce a shear, although the obtained coupling factors distinctly deviated from the coupling factor calculated according to the tangent rule.

8.2. Mobility of stress driven boundaries, its dependence on temperature and misorientation

Measurements on bicrystals with various grain boundaries performed at different elevated temperatures revealed that stress driven shear-coupled boundary migration is thermally activated, and the boundary migration rate v depends on temperature according to an Arrhenius relation $v = v_0 exp(-H/kT)$, where H is the activation enthalpy of grain boundary migration. Figure 13b depicts the misorientation dependence of the migration activation enthalpy for <100> tilt boundaries [18]. As seen, in both low angle regimes (θ < 18° and θ > 76°) the measured activation enthalpy remains virtually the same with a value of about H=1.45 eV. In the high angle regime, however, the migration activation enthalpy changes with the angle in a non-monotonic fashion, such that the lower H values correspond to boundaries with misorientations close to low Σ CSL orientation relationships (Fig. 13b). This suggests that the migration mechanism, which is reflected in the migration activation enthalpy, remains essentially unaltered for all low angle boundaries, whereas it varies substantially with the character of structurally different high angle boundaries.

8.3. Stress driven migration of Σ7 tilt boundary in Al

An unexpected boundary behavior under an applied stress was observed in experiments with Σ7 tilt boundaries [21,67]. Specifically, three symmetrical tilt grain boundaries with misorientations close to 38.2°<111>, 73.4°<201> and 135.6°<112>, i. e. the same special Σ7{132} CSL boundary, were examined. The experiments showed that the boundaries in the investigated bicrystals moved under an applied stress, but their migration was not accompanied by a shear strain, i.e. tangential displacement of the adjacent grains. This result provides evidence that the migration behavior of high angle low Σ grain boundaries under stress can differ from that of random boundaries, and their stress driven migration must not necessarily be coupled to shear, as predicted by the geometrical models of stress induced boundary migration.

Crystallographically equivalent boundaries in bicrystals of different geometric description behaved differently with respect to the migration rate and its temperature dependence [21]. The migration activation enthalpy ranged from 0.7 to 1.3 eV. This reveals that the kinetics of stress driven boundary migration and its operative mechanism depend on the direction of the applied stress.

8.4. Concurrent grain boundary motion and grain rotation

The remarkable boundary response to an applied stress – boundary migration accompanied by both a translation of the adjacent grains parallel to the boundary plane and their rotation around the boundary plane normal was observed in experiments with a 18.2°<100> mixed tilt-twist grain boundary [24]. This boundary was composed of a rotation angle θ = 18.2° around a common [001] axis and grain boundary plane rotated by 20° with respect to the tilt boundary plane, i.e. it had a twist component ξ = 20°.

The observed behavior was quantitatively characterized by measuring the surface topography of the bicrystal by means of atomic force microscopy after annealing under stress (Fig. 14). The topographic

profiles across the boundary measured on the opposite sample surfaces clearly evidenced that the surface of the shrinking crystal (grain 2) after annealing was rotated around the boundary normal. Also, from the measured topography it is apparent that this rotation proceeded simultaneously with the normal boundary displacement (Fig. 14), providing evidence that the two processes were related.

The results of this experiment can be rationalized in terms of the dislocation structure of the mixed boundary, which is assumed to contain a set of edge dislocations accommodating the tilt component of the misorientation and a set of screw dislocations accommodating the twist component. Under the applied stress edge dislocations move in the direction normal to the boundary plane and produce shear deformation of the lattice and, therefore, the coupled boundary motion. At the same time, the applied stress imposes Peach-Kohler forces on the screw dislocations causing their glide in the boundary plane. This process induces grain rotation, the sign of which depends on the direction of the shear stress. It is noteworthy that this grain rotation changes the twist component of the grain misorientation (increases or decreases), demonstrating the important effect of changing the grain boundary character by applied stresses.

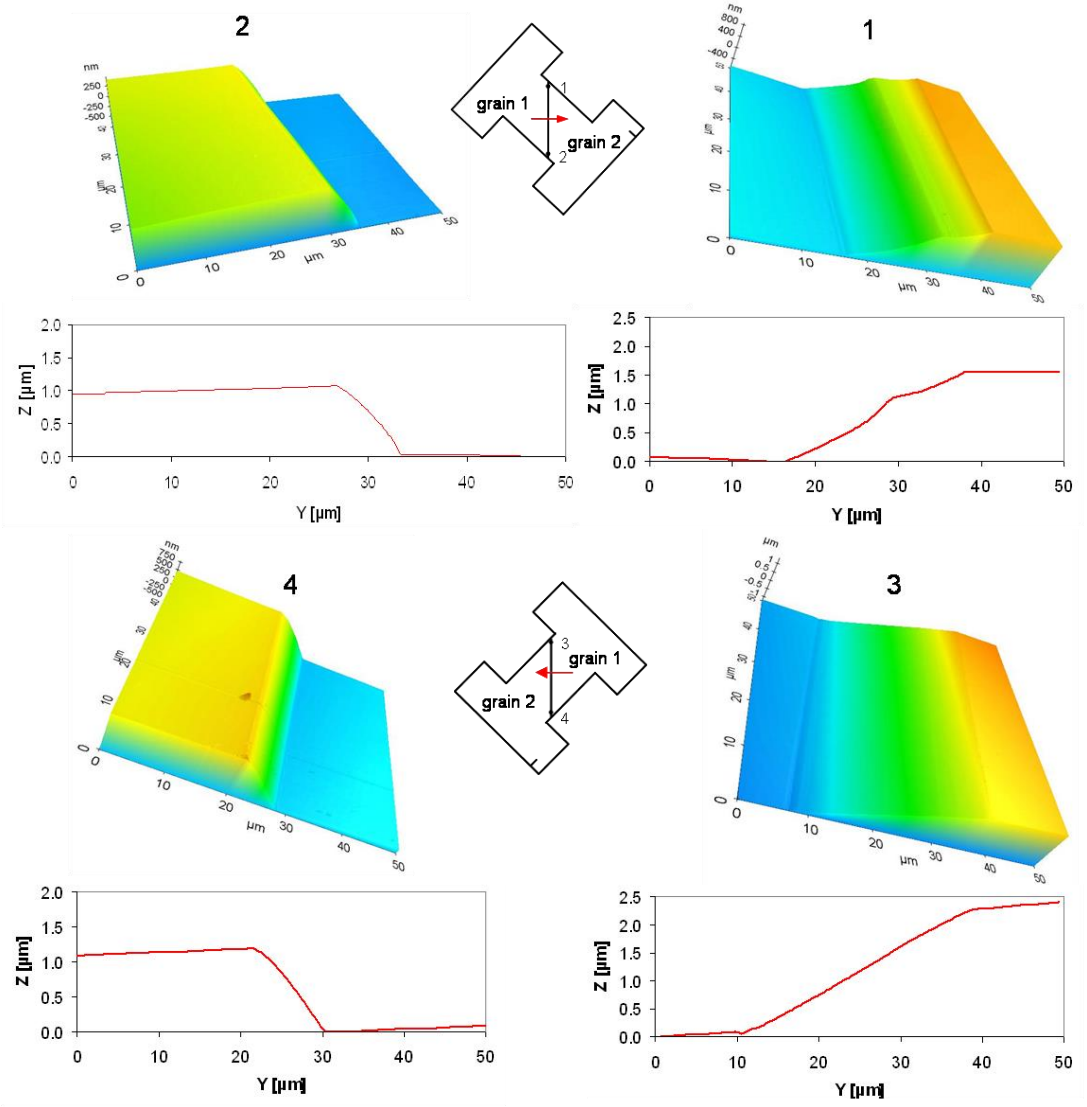

Figure 14 Surface topography of the bicrystal with 18.2° <100> mixed tilt-twist (ξ = 20°) boundary after annealing at 392°C under applied tensile stress of 0.23 MPa [24].

Acknowledgements
The authors express their gratitude to the Deutsche Forschungsgemeinschaft (DFG) for financial support (Grants MO 848/10, MO 848/14).

References
[1] Harris KE, Singh VV and King AH 1998 *Acta Mater.* **46** 2623
[2] Klinger L and Rabkin E 2011 *Acta Mater.* **59** 6691
[3] Bachurin DV, Nazarov AA and Weissmüller J 2012 *Acta Mater*. **60** 7064
[4] Ashkenazy Y, Averback RS and Albe K 2001 *Phys. Rev. B* **64** 205409
[5] Haslam AJ, Phillpot SR, Wolf D, Moldovan D and Gleiter H 2001 *Mater. Sci. Eng.* A **318** 293
[6] Upmanyu M, Srolovitz DJ, Lobkovsky AE, Warren JA and Carter WC 2006 *Acta Mater.* 54 1707
[7] Cahn JW and Taylor JE 2004 *Acta Mater.* **52** 4887
[8] Cahn JW, Mishin Y and Suzuki A 2006 *Acta Mater.* **54** 4953
[9] Cahn JW, Mishin Y and Suzuki A 2006 *Philos. Mag.* **86** 3965
[10] Ivanov VA and Mishin Y 2008 *Phys. Rev. B* **78** 064106
[11] Caillard D, Mompiou F and Legros M 2009 *Acta Mater.* **57** 2390
[12] Mompiou F, Legros M and Caillard D 2009 *Acta Mater.* **58** 3676
[13] Khater HA, Serra A, Pond RC and Hirth JP 2012 *Acta Mater.* **60** 2007
[14] Rajabzadeh A, Mompiou F, Legros M and Combe N 2013 *Phys. Rev. Letters* **110** 265507
[15] Taupin V, Capolungo L and Fressengeas C 2014 *Int. J. Plast.* **53** 179
[16] Molodov DA, Ivanov VA and Gottstein G 2007 *Acta Mater.* **55** 1843.
[17] Molodov DA, Gorkaya T and Gottstein G 2007 *Mater. Sci. Forum* **558-559** 927
[18] Gorkaya T, Molodov DA and Gottstein G 2009 *Acta Mater*. **57** 5396
[19] Gorkaya T, Burlet T, Molodov DA and Gottstein G 2010 *Scripta Mater* **63** 633
[20] Molodov DA, Gorkaya T and Gottstein G 2011 *J. Mat. Sci.* **46** 4318
[21] Molodov DA, Gorkaya T and Gottstein G 2011 *Scripta Mater*. **65** 990
[22] Rajabzadeh A, Legros M, Combe N, Mompiou F and Molodov DA 2013 *Philos. Magazine* **93** 1299
[23] Rajabzadeh A, Mompiou F, Lartigue-Korinek S, Combe N, Legros M and Molodov DA 2014 *Acta Mater.* 77 223
[24] Gorkaya T, Molodov KD, Molodov DA and Gottstein G 2011 *Acta Mater.* **59** 5674
[25] Smoluchowski R 1951 *Phys. Rev.* **83** 69
[26] Turnbull D 1951 *Journal of Metals* **3** 661
[27] Vandermeer RA 1965 *Transactions AIME* **233** 266
[28] Vandermeer RA, Juul-Jensen D and Woldt E 1997 *Metall. Mater. Trans. A* **28** 749
[29] Aristov V Y, Fradkov VE and Shvindlerman LS 1979 *Phys. Met. Metall.* **45** 83
[30] Molodov DA, Gottstein G, Heringhaus F and Shvindlerman LS 1998 *Acta Mater.* **46** 5627
[31] Günster Ch, Molodov DA and Gottstein G 2013 *Acta Mater.* **61** 2363
[32] Gottstein G, Molodov DA and Shvindlerman LS 2010 *ASM Handbook* vol 22B, ed DU Furrer and SL Siemiatin (Materials Park: ASM International) p 67
[33] Sutton AP and Balluffi RW 1995 *Interfaces in Crystalline Materials* (Oxford: Clarendon Press)
[34] Hsieh TE and Balluffi RW 1989 **37** 2133
[35] Straumal BB, Polyakov SA, Bischoff E, Gust W and Mittemeijer EJ 2001 *Interface Science* **9** 287
[36] Lee SB, Sigle W and Rühle M 2003 *Acta Mater.* **51** 4583
[37] Rohrer GS 2005 *Annu. Rev. Mater. Res.* **35** 99
[38] Rohrer GS 2011 *J. Mater. Sci.* **46** 5881
[39] D. Y. Yoon, and Y. K. Cho 2005 *J Mater Sci*, **40**, 861-870.
[40] Molodov DA, Günster Ch, Gottstein G and Shvindlerman LS 2012 *Philos. Magazine* **92** 4588
[41] Straumal BB, Rabkin E, Sursaeva VG and Gornakova AS 2005 *Zt. Metallkd.* **96** 161

[42] Straumal BB, Sursaeva VG and Gornakova AS 2005 *Zt. Metallkd.* **96** 1147
[43] Sursaeva VG, Straumal BB, Gornakova, Shvindlerman LS and Gottstein G 2008 *Acta Mater.* **56** 2728
[44] Sursaeva VG 2010 *Materials Letters* **64** 105
[45] Brandenburg J-E, Barrales-Mora LA, Molodov DA and Gottstein G 2013 *Acta Mater.* **61** 5518.
[46] Lee SB, Yoon DY and Henry MF 2000 *Acta Mater.* **48** 3071
[47] Lee SB, Hwang NM, Yoon DY and Henry MF 2000 *Metall. Mater. Trans. A* **31** 985
[48] Kazaryan A, Wang Y, Dregia SA and Patton BR 2002 *Acta Mater.* **50** 2491
[49] Rabkin E 2005 *J. Mater. Sci*. **40** 875
[50] Kang S-JL, Lee MG, and An SM 2009 *J. Am. Ceram. Soc.* **92** 1464
[51] Kirch DM, Zhao B, Molodov DA and Gottstein G 2007 *Scripta Mater.* **56** 939
[52] Kirch DM, Jannot E, Barrales-Mora LA, Molodov DA, Gottstein G 2008 *Acta Mater.* **56** 4998
[53] Brandenburg J-E, Barrales-Mora LA, Molodov DA and Gottstein G 2013 *Scripta Mater.* **68** 980
[54] Brandenburg J-E, Barrales-Mora LA and Molodov DA 2014 *Acta Mater.* **77** 294
[55] Verhasselt JCh, Gottstein G, Molodov DA and Shvindlerman LS 1999 *Acta Mater.* **47** 887
[56] Surholt T, Molodov DA and Herzig Chr 1998 *Acta Mater.* **46** 5345
[57] Molodov DA, Czubayko U, Gottstein G and Shvindlerman LS 1995 *Scripta Metall. Mater.* **32** 529
[58] Gottstein G, Molodov DA, Czubayko U and Shvindlerman LS 1995 *J. de Phys. IV* **5** 89
[59] Molodov DA, Czubayko U, Gottstein G and Shvindlerman LS 1998 *Acta Mater.* **46** 553
[60] Gottstein G, Molodov DA and Shvindlerman LS and Srolovitz DJ 2001 *Curr. Opin. Solid State Mater. Sci.* **5** 9
[61] Ivanov VA, Molodov DA, Shvindlerman LS and Gottstein 2004 *Mater. Sci. Forum* **467-470** 751
[62] Ivanov VA, Molodov DA, Shvindlerman LS and Gottstein G 2004 *Acta Mater.* **52** 969
[63] Furtkamp M, Gottstein G, Molodov DA, Semenov VN and Shvindlerman LS 1998 *Acta Mater.* **46** 4103
[64] Kirch DM, Ziemons A, Burlet T, Lischewski I, Molodova X, Molodov DA and Gottstein G 2008 *Rev. Sci. Instrum.* **79** 043902
[65] Molodov DA and Mishin Y 2013 *Microstructural Design of Advanced Engineering Materials*, ed DA Molodov (Weinheim: Wiley-VCH) p 201
[66] Gorkaya T, Burlet T, Molodov DA and Gottstein G 2012 *Mater. Sci. Forum* **715-716** 819
[67] Molodov DA, Gorkaya T and Gottstein G 2012 *Mater. Sci. Forum* **706-709** 2886
[68] Lee B-J and Choi S-H 2004 *Modelling Simul. Mater. Sci. Eng.* **12** 621
[69] Lee B-J and Baskes MI 2000 *Phys. Rev. B* **62** 8564
[70] Lee B-J, Baskes MI, Kim H and Cho YK 2001 *Phys. Rev. B* **64**:184102
[71] Lee B-J, Shim J-H and Baskes MI 2003 *Phys. Rev. B* **68** 144112
[72] Plimpton SJ 1995 *Comput. Phys.* **117** 1
[73] Janssens KGF, Olmsted D, Holm EA, Foiles SM, Plimpton SJ and Derlet PM 2006 *Nature Materials* **5** 124
[74] Huang Y and Humpreys FJ 2000 *Acta Mater*. **48** 2017
[75] Yang CC, Rollett AD and Mullins WW 2001 *Scripta Mater*. **24** 2735
[76] Viswanathan R and Bauer CL 1973 *Acta Metall*. **21** 1099
[77] Barrales-Mora LA, Brandenburg J-E and Molodov DA 2014 *Acta Mater.* **80** 141
[78] Srinivasan SG and Cahn JW 2002 *Science and technology of interfaces,* ed S Ankem, CS Pande, I Ovidko and R Ranganathan (Seattle: TMS) p 3
[79] Trautt ZT and Y Mishin 2012 *Acta Mater.* **60** 2407
[80] Wu KA and Voorhees PW 2012 *Acta Mater.* **60** 407
[81] Mompiou F, Legros M, Radetic T, Dahmen U, Gianola DS and Hemker KJ 2012 *Acta Mater.* **60** 2209
[82] Babcock SE and Balluffi RW 1989 *Acta Metall.***37** 2367

[83] Radetic T, Ophus C, Olmsted DL, Asta M and Dahmen U 2012 *Acta Mater.* **60** 7051
[84] Read WT and Shockley W 1950 *Phys. Rev.* **78** 275
[85] Washburn J and Parker ER 1952 *Trans AIME* **194** 1076
[86] Li CH, Edwards EH, Washburn J and Parker ER *Acta Metall.* 1953 **1** 223
[87] Bainbridge DW, Li CH and Edwards EH 1954 *Acta Metall.* **2** 322
[88] Watanabe T, Kimura SI and Karashima S 1984 *Philos. Mag. A* **49** 845
[89] Horiuchi R, Fukutomi H and Takahashi T 1987 *Fundamentals of Diffusion Bonding*, ed Y Ishida (Amsterdam: Elsevier) p 347
[90] Fukutomi H and Kamijo T 1985 *Scripta Metall.* **19** 195
[91] Fukutomi H, Iseki T, Endo T and Kamijo T 1991 *Acta Metall. Mater.* **39** 1445
[92] Sheikh-Ali AD and Valiev RZ 1990 *Phys Status Solidi (a)* **117** 429
[93] Sheikh-Ali AD, Lavrentyev FF and Kazarov YuG 1997 *Acta Mater.* **45** 4505
[94] Sheikh-Ali AD and Szpunar JA 1998 *Mater. Sci. Eng.* **A245** 49
[95] Yoshida H, Yokoyama K, Shibata N, Ikuhara Y and Sakuma T 2004 *Acta Mater.* **52** 2349
[96] Suzuki A and Mishin Y 2005 *Mater. Sci. Forum* **502** 157
[97] Mishin Y, Suzuki A, Uberuaga BP and Voter AF 2007 *Phys. Rev. B* **75** 224101
[98] Zhang H, Du D and Srolovitz DJ 2008 *Philos. Magazine* **88** 243
[99] Lim AT, Haataja M, Cai W and Srolovitz DJ 2012 *Acta Mater.* **60** 1395
[100] Legros M, Gianola GS and Hemker KJ 2008 *Acta Mater.* **56** 3380
[101] Rupert TJ, Gianola DS, Gan Y and Hemker KJ 2009 *Science* **326** 1686
[102] Mompiou F, Caillard D and Legros M 2009 *Acta Mater.* **57** 2198